Phonon-mode-specific lattice dynamical coupling of carriers in semiconductors using Raman and optical spectroscopic techniques

Omkar V. Rambadey ⓘ, Minal Gupta ⓘ, and P. R. Sagdeo ⓘ*

Materials Research Laboratory, Indian Institute of Technology Indore, Indore 453552, India

We demonstrate a methodology for quantitative estimation of electron-phonon coupling (EPC) for each phonon mode taking base from second-order correction in polaron-energy resulting bandgap renormalization of the semiconductor by treating EPC as perturbation. This gives coupling constant (α_p) for the pth phonon mode in terms of phonon energy and renormalized bandgap due to EPC. These theoretical inferences are experimentally explored using combination of optical absorption and Raman spectroscopies for Γ phonons of temperature-varied GaN and TiO_2; results reveal a systematic enhancement in α_p with temperature that exhibits unique percent variation of α_p for each mode. A higher percent change is observed for the mode known to exhibit greater coupling strength, thereby supporting the theoretical discussions. In this paper, we provide a simpler method to directly probe quantum level phonon-specific interactions with electrons, otherwise probed with much advanced techniques.

I. INTRODUCTION

The interaction of charge carriers with phonons is one of the most important problems in condensed matter physics [1]. In this direction, in their pioneering reviews, Ziman [1] and Giustino [2] suggest the significance of electron-phonon interactions in understanding systems such as multifunctional, topological, and superconducting materials. It is important to note that the emergence of superconductivity via electron-phonon coupling (EPC) [3] has initiated intense research in view of understanding the physics of EPC [4–6]. Furthermore, it is known that the electrical properties in metallic and semiconductor materials at high temperature are largely governed by EPC [7–9]. Therefore, it is necessary to quantitively understand the phenomenon of EPC. This problem is mathematically treated by considering the interference between the (discrete) phonons and (continuum) electrons lying in the same energy spread [10,11]. As the number density, energy spread, position, and direction of vibration of each phonon mode is different, hence, it is natural to except that not all phonons will equally interfere with the electronic continuum, thereby exhibiting unique coupling strengths which is also evident from earlier efforts by researchers [12–14]. The importance of this inference may lie in the fact that, due to the exclusive coupling strengths of individual modes, only certain phonons may be responsible for the attractive interaction between electrons in superconductors. In addition, the scattering processes in metals and semiconductors that explain their resistivity may have a correlation with the phonon-mode-specific interaction with electrons. Thus, understanding the selective contributions of each phonon in EPC could be important to tune electrical properties of these applied materials

such that the selective excitation of phonons by some suitable external perturbations may lead to tuning of the superconducting transition at higher temperatures, and similarly, the electrical properties of semiconductors may also be controlled by the knowledge of coupling strength of each phonon mode. In this direction, various experimental techniques have been utilized by different groups, viz., angle resolved photoelectron spectroscopy [15], femtosecond x-ray diffraction [16], inelastic He-atom scattering [17], and resonant inelastic x-ray scattering [18]; however, it is noteworthy that such highly specialized techniques are not widely accessible, and most importantly, the coupling strength is determined indirectly by means of fitting the experimental data with a specific theoretical model.

In this paper, thus, we present an attempt to quantitatively characterize such mode-selected EPC in semiconductors by simultaneous application of two simpler widely accessible techniques—Raman and optical absorption spectroscopies—to extract the information of coupling strength for individual Γ-point phonons. The theoretical motivation of this paper is related to analytically approaching the polaron (electron-bounded phonon cloud) energy in a system and correlating it with the optical bandgap of the semiconductor. This gives the following final relation between the energy ($\hbar\omega_p$) associated with the pth phonon mode and variation in the bandgap (ΔE_g) due to the renormalization in view of the EPC: $\Delta E_g \sim \alpha_p \hbar\omega_p$; here, α_p represents the effective coupling constant for the pth phonon mode. Certainly, the quantity α_p would strongly depend on the density of states (DOS) of the interacting electrons and phonons, such that the greater the overlap between the states, the stronger the coupling would be, as shown in Fig. 1(a). In addition, the polaron picture vividly visualizes the influence of an electron on the nearby ions such that it would more affect the out-of-phase vibrations, thus, the optical phonons, and in even that, the preferential participation
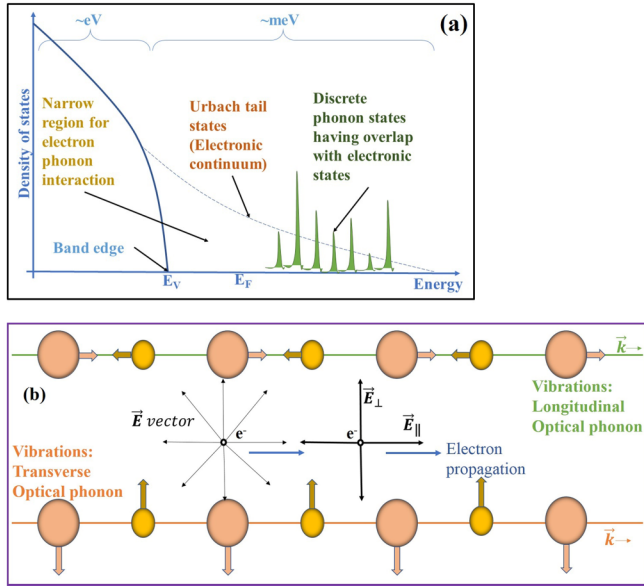
FIG. 1. (a) Schematic representation for describing the preference of certain phonons toward discrete-continuum interference. E_V and E_F are the valence band maximum and Fermi level, respectively. (b) Representative for describing the preference of longitudinal optical (LO) phonons toward electron-phonon interactions.

of longitudinal optical (LO) phonons in the coupling could also be realized. For an electron passing through a certain region in the lattice, the component of its electric field ($\vec{E}$) along the propagation vector of phonons $\vec{k}$ (or $\vec{E} \cdot \vec{k}$, having dimensions of volts/length^2) may be understood as an effective potential over the vibrating atoms/ions imparted along the cross-section in the region where the electron moves. Here, it could be realized for the ions exhibiting longitudinal vibrations that their amplitudes/displacements are always along both $\vec{E}_\parallel$ and $\vec{k}$ vectors, $\vec{E}_\parallel$ denoting the electric field component due to the presence of the electron along $\vec{k}$, and $\vec{E}_\perp$ being perpendicular to it. Thus, it could be inferred that, in such a case, LO phonons may get affected to a greater extent. This discussion is picturized in Fig. 1(b).

Further, these results have been realized by following the mathematical approach provided in earlier reports [19–21] which, under the assumption that a variation in EPC strength should also introduce some variation in the optical bandgap, yielded the aforementioned relationship. To further investigate the experimental aspect of such a correlation, single-crystal GaN (direct bandgap) and polycrystalline TiO$_2$ (indirect bandgap) samples have been considered, keeping in view the importance of these semiconductors from the point of application as well as fundamental studies [22–31].

Hence, in this paper, *in situ* temperature-dependent (TD) Raman and optical absorption spectroscopy experiments have been performed on the GaN and TiO$_2$ samples to get the values of the bandgap and phonon energy. The extracted quantities ΔE_g (change in bandgap in considered temperature interval) and $\hbar\omega_p$ have been further utilized to obtain the information of temperature variation of coefficient α. Since this coefficient describes the effective coupling constant [32] whose magnitude could be a function of the overlapping DOS

of the interacting electrons (e) and phonons (ph), its importance may be realized for probing phonon-mode-specific EPC in relevant semiconductors. As the information of the overlapping DOS of e-ph could not be achieved directly, the final inferences have been made through the percent change of experimentally observed α within the varying range of the perturbing parameter (temperature, in this case). The different percent variations for each phonon mode can be interpreted as a distinct evolution of the overlapping DOS and hence the specific EPC strength for that phonon mode. Therefore, this paper may be helpful in determining the mode-selected coupling strength via utilizing conventional Raman and optical absorption spectroscopy techniques. In this paper, we provide a very important aspect of fundamental science in view of probing the quantum level interactions between lattice vibrations (phonons) and electrons in semiconductors specific to a symmetry element.

II. MATERIALS AND METHODS

For the experimental investigation of the theoretical discussions, a procured single-crystal GaN [002] sample and polycrystalline TiO$_2$ in powdered form have been considered for the measurements. To probe the temperature dependence of the optical bandgap of the samples, we opted for *in situ* diffuse reflectance spectroscopy [33] with the help of an ultraviolet-visible-near infrared spectrometer [33–35], attached with an in-house-developed temperature-control setup [36]. Moreover, the TD Raman spectra have been collected using a high-resolution dispersive spectrometer equipped with a 633 nm excitation laser source with a charge-coupled device detector in backscattered mode [37,38]. The laser was focused on the sample with the help of a $50\times$ magnification glass compensating objective [39,40]. To vary the sample temperature, a temperature control stage having an accuracy of the order of 0.1 K was utilized [41,42].

III. THEORETICAL BACKGROUND—BANDGAP, PHONON FREQUENCY, AND COUPLING STRENGTH

We consider an ionic lattice network where a nonrelativistic electron with mass μ interacts with the quantized scalar field of phonons, thereby forming a polaron in that region. The system could be realized through the kinetic energy of an electron and the vibrational energies of phonons in the vicinity of that electron, which may have a dispersion in their momenta. In addition, there would exist such phonons that could couple with the electron. Thus, the Hamiltonian of this system may be represented as [20,21,32]

$$H = -\frac{\hbar^2}{2\mu}\Delta + \hbar\sum_k \omega_k a_k^\dagger a_k$$
$$+ \frac{g}{\sqrt{V}}\sum_k [A_k \exp(ikr)a_k + A_k^*\exp(-ikr)a_k^\dagger]. \quad (1)$$

The terms a_k and a_k^+ correspond to the creation and annihilation operators for phonons associated with frequency ω_k and momentum k. Here, V corresponds to the system volume, and the coefficients A_k denote the Fourier components for the source density. The first two terms in Eq. (1) describe the part

of the noninteracting electron-phonon (e-ph), and the third term accounts for the coupled e-ph. Further, considering the conservation of total momentum of the polaron, one could express the total momentum P as [20] $P = -i\hbar\nabla + \sum_k \hbar k a_k^\dagger a_k$; therefore, it may be possible to perform a canonical transformation of the kind:

$$H \rightarrow SHS^\dagger, \text{ such that } S = \exp\left(-i\mathbf{r}\sum_k k a_k^\dagger a_k\right), \quad (2)$$

which gives the Hamiltonian infollowing form [20]:

$$H = \frac{1}{2\mu}\left(P - \sum_k \hbar k a_k^\dagger a_k\right)^2 + \hbar\sum_k \omega_k a_k^\dagger a_k$$
$$+ \frac{g}{\sqrt{V}}\sum_k\left(A_k a_k + A_k^* a_k^\dagger\right). \quad (3)$$

Further, following the theory of the optical polaron [20,32], where the phonon frequency is assumed to be wave vector independent, we have

$$\omega_k = \omega \text{ and } gA_k = -i\frac{\hbar\omega}{k}\left(\frac{\hbar}{2\mu\omega}\right)^{1/4}(4\pi\alpha)^{1/2}. \quad (4)$$

Here, α $(0 < \alpha < 1)$ denotes a dimensionless coupling constant. On incorporating the forms of ω_k and gA_k from Eq. (4) into Eq. (1), the Hamiltonian becomes [20,32]

$$H = \left[\left(\frac{P}{\sqrt{2\mu}} - \frac{\hbar}{\sqrt{2\mu}}\sum_k k a_k^\dagger a_k\right)^2 + \hbar\omega\sum_k a_k^\dagger a_k\right]$$
$$+ \left[-i\hbar\omega\left(\frac{\hbar}{2\mu\omega}\right)^{1/4}\sqrt{\frac{4\pi\alpha}{V}}\sum_k\frac{1}{k}\left(a_k - a_k^\dagger\right)\right] \quad (5)$$

Here, P is the total polaron momentum. The first two terms collectively can be seen as H_0 (non-interacting Hamiltonian), and the latter term as H_{ep} that describes the interacting electrons and phonons whose interaction strength may be associated with the coefficient α. At this point, H_{ep} could be seen as the perturbation that brings the interaction between the electron and phonon; thus, the *ground state Hamiltonian at small momenta* may be expressed as [20]

$$\xi \sim \mathcal{E} + \left(\frac{P}{\sqrt{2\mu}}\right)^2\frac{\mu}{m} + O\left[\left(\frac{P}{\sqrt{2\mu}}\right)^4\right], \quad (6)$$

where $\mathcal{E}$ is the ground state energy of the polaron at rest, m is the polaron effective mass, and the energy eigenvalue for the ground state will be [20]

$$E_0^{(0)} = \frac{P^2}{2\mu}, \quad (7)$$

which may be interpreted as the kinetic energy of a free electron with mass μ and momentum P. Thus, it reflects the fact that, in the ground state, both the polaron and electron momenta resemble each other. However, due to the perturbation manifesting as the term H_{ep} in Eq. (5), the ground state energy may acquire certain modifications. In that view, the first-order $[E_0^{(1)}]$ and second-order $[E_0^{(2)}]$ corrections in accordance

with the perturbation theory (PT) could be realized as the following [20]:

$$E_0^{(1)} = \langle n_k|H_{ep}|n_k\rangle, \quad (8)$$

$$E_0^{(2)} = \sum_{n,\,n\neq 0}\sum_{k'=1}^n\frac{|\langle n_k|H_{ep}|n_{k'}\rangle|^2}{E_k^{(0)} - E_{k'}^{(0)}}. \quad (9)$$

It is noteworthy from Eqs. (8) and (9) that the terms corresponding to the correction $E_0^{(1)}$ would vanish, as evident from the form of H_{ep} defined in Eq. (5), leaving the higher-order correction $E_0^{(2)}$ to be nonzero. Therefore, it may be inferred that the second-order correction in the PT corresponds to the first-order correction in the polaron model. Now referring to Eq. (9), all those states $(|n_k\rangle)$ differing by unity would contribute to nonzero outcomes under the correction $E_0^{(2)}$; in other words, for the states with n_k phonons having momentum k, a nonvanishing outcome would be obtained if $\Delta n_k = \pm 1$. Here, the denominator contains the propagator terms that would correspond to the transition of the system from the vacuum state of a free electron to the state with n phonons having total momenta nk. Therefore, for the transition from the ground state $|0\rangle$ to some state $|n_k\rangle$, the propagator term may be given as [20]

$$E_0^{(0)} - E_n^{(0)} = \sum_{n=1}^n n\hbar\omega - 2\frac{P}{2\mu}\sum_{n=1}^n n\hbar k + \frac{1}{2\mu}\left(\sum_{n=1}^n n\hbar k\right)^2. \quad (10)$$

Let us denote the total momentum for a given state n with k momenta as $nk = k_i$, where the index i would run from 1 to n. Also, let the total number of phonon states $\sum_{n=1}^n n$ be represented by n. Then Eq. (10) would simplify to the following form [20]:

$$E_0^{(0)} - E_n^{(0)} = n\hbar\omega - 2\frac{P}{2\mu}\sum_{i=1}^n k_i + \frac{1}{2\mu}\left(\sum_{i=1}^n k_i\right)^2. \quad (11)$$

Hence, utilizing the propagator terms from Eq. (11) into Eq. (9), the first-order correction (in the polaron model) in the ground state energy of the system will be [20]

$$E_0^{(2)}|_{n=1} = -(\hbar\omega)^2\left(\frac{\hbar}{2\mu\omega}\right)^{1/2}\frac{\alpha}{2\pi^2}\int\frac{1}{k^2}$$
$$\times\frac{1}{\hbar\omega - 2\frac{P}{2\mu}\hbar k + \frac{\hbar^2 k^2}{2\mu}}dk, \quad (12)$$

or

$$E_0^{(2)}|_{n=1} = -\hbar\omega\left(\frac{\hbar}{2\mu\omega}\right)^{1/2}\frac{\alpha}{2\pi^2}\int\frac{1}{k^2}$$
$$\times\frac{1}{1 - 2\frac{P}{2\mu\hbar\omega}\hbar k + \frac{\hbar^2 k^2}{2\mu\hbar\omega}}dk. \quad (13)$$

Here, the summation has been transformed into integration over momenta. The solution of the integral in Eq. (13) for

small momenta may be obtained to be [20,32]

$$E_0^{(2)}|_{n=1} = -\hbar\omega \frac{\alpha}{\left(\frac{P}{\sqrt{2\mu\hbar\omega}}\right)} \sin^{-1}\left(\frac{P}{\sqrt{2\mu\hbar\omega}}\right)$$

$$\sim -\hbar\omega\alpha\left\{1 + \frac{1}{6}\left(\frac{P}{\sqrt{2\mu\hbar\omega}}\right)^2 + O\left[\left(\frac{P}{\sqrt{2\mu\hbar\omega}}\right)^4\right]\right\}$$

(14)

Further, the energy of polaron after correction would be given as

$$E = E_0^{(0)} + E_0^{(2)}|_{n=1}$$

$$= \frac{P^2}{2\mu} - \alpha\hbar\omega\left\{1 + \frac{1}{6}\left(\frac{P}{\sqrt{2\mu\hbar\omega}}\right)^2 + O\left[\left(\frac{P}{\sqrt{2\mu\hbar\omega}}\right)^4\right]\right\}$$

(15)

or

$$E = E_0^{(0)} + E_0^{(2)}|_{n=1}$$

$$= -\alpha\hbar\omega + \left(1 - \frac{\alpha}{6}\right)\left(\frac{P}{2\mu}\right)^2 + O\left[\left(\frac{P}{2\mu}\right)^4\right].$$

(16)

The comparison of the first term in the right-hand side of Eq. (16) with Eq. (6) gives the following relation for $\mathcal{E}$ in terms of the coupling constant [19,20]:

$$\mathcal{E} = -\alpha\hbar\omega.$$

(17)

Now the electron-phonon interactions are not only expected to alter the phonons but also the electronic structure due to the discrete (phonon)–(electronic) continuum interference that may lead to the optical bandgap renormalization, also evident from earlier reports on the estimation of EPC using bandgap renormalization [6,43,44]. It should be noted that the bandgap is dependent on the lattice parameters which could be a function of the external perturbation. Thus, the ultimate consequence could be the modification in the orbital overlapping among the constituent atoms that may lead to the modification in the DOS and hence the strength of the EPC [45]. Therefore, the energy $\mathcal{E}$ may be expected to contribute toward the optical bandgap renormalization of the semiconductor due to electron-phonon interactions [43,46]. Hence, the change in optical bandgap may have a possible correlation with the associated coupling between the pth phonons and electrons that form the absorption edge in semiconductors [47]. Thus, by that consideration [20,48],

$$\Delta E_g \sim \alpha_p \hbar\omega_p.$$

(18)

This expression imparts the information of EPC strength associated with a given phonon mode in altering the optical bandgap of the semiconductor sample, i.e., the contribution from each phonon mode (characterized by its frequency ω_p) in the renormalization of the bandgap may be different which could be ascribed to the specific EPC strength ($\sim\alpha_p$) associated with that phonon. Additionally, it should be noted that the coupling strength would be a function of the DOS of the interacting electrons and phonon [49]; however, the direct information of these DOSs may not be possible to achieve
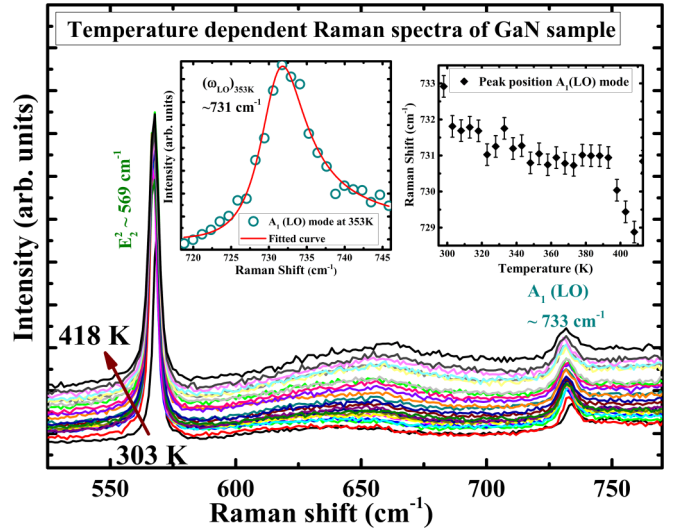
FIG. 2. Temperature-dependent Raman spectra of GaN sample; inset shows schematic representation for the fitted curve along the $\sim 733\,\mathrm{cm}^{-1}$ $A_1(\mathrm{LO})$ mode and the obtained peak position at 353 K.

efficiently [refer to Fig. 1(a)]. Nonetheless, the evolution of the overlapping (interacting) DOS may be realized via varying the external perturbation on the system. Hence, to experimentally investigate these inferences, the TD behavior of the considered samples has been investigated, keeping in view the consequent alteration in the DOS of interacting electrons and phonons, thus the coupling strength and hence the bandgap due to the scaling of temperature [46]. Therefore, a detailed experimental investigation has been provided in view of the final relation obtained in Eq. (18) in upcoming sections.

IV. EXPERIMENTAL STUDIES ON BANDGAP AND PHONON FREQUENCIES

A. TD Raman spectra—GaN

As we aim to study the phonon-mode-specific EPC in a semiconductor system, it is necessary to set an external perturbing parameter that could alter the strength of EPC; for that, the sample temperature could be a suitable quantity since the strength of EPC has been known to exhibit thermal dependence as well [8,47]. Therefore, the TD Raman spectra of GaN and TiO$_2$ may be expected to exhibit a signature of EPC that is of interest for the present context. In that view, Raman spectra for GaN have been collected in the temperature range $\sim$300–420 K, shown in Fig. 2.

The Raman modes $\sim$569 and 733 cm^{-1} could be identified as E_2^2 and $A_1(\mathrm{LO})$ symmetries, respectively. Moreover, a bandlike feature could also be observed around the region $\sim 650\,\mathrm{cm}^{-1}$ which does not belong to the point group symmetry of GaN [50]; thus, its appearance may be ascribed to the crystal imperfections that may have developed during the preparation of the GaN sample. In addition, it is noteworthy that the $A_1(\mathrm{LO})$ mode exhibits an asymmetric line shape for the considered sample; such asymmetry was not observed by earlier authors [26,50]. In that case, this observed feature may be understood in terms of the contribution from the disorder due to lattice imperfections [51] that may possibly
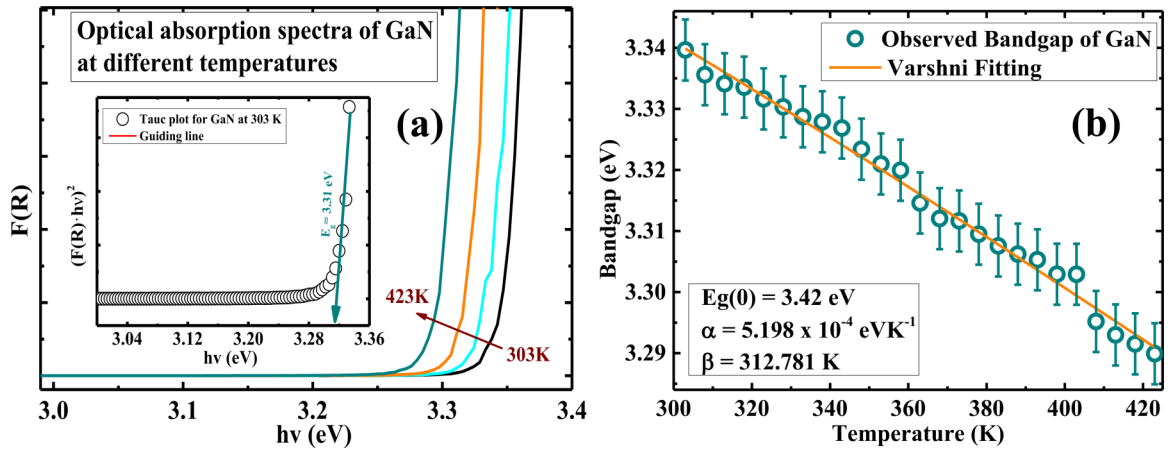
FIG. 3. (a) Schematic for the optical absorption spectra recorded for GaN single crystal sample at 300 K; inset shows schematic for the Tauc plot obtained at 303 K. (b) Plot for temperature variation of bandgap in GaN single crystal sample, fitted with Varshni relation.

add to the electron-phonon interactions [47] which could explain the observed feature in the Raman spectra. Nevertheless, a schematic representation for the fitted Raman mode $\sim 733\,\mathrm{cm}^{-1}$ has also been shown in the inset of Fig. 2. A schematic for the temperature variation of the peak position of the A_1(LO) mode has also been shown in the inset of Fig. 2. Clearly, a systematic redshift could be seen in the peak position attributing to the thermal effects [42,52]. Further, since the thermal variation in the Raman modes may arise due to different phonon processes that may not have identical impacts on each mode [53]; different Raman modes may exhibit nonidentical thermal responses, in which one factor related to the interaction with electrons could also be involved. Hence, with that consideration, it may be inferred that interaction of these phonons with electrons may also affect the electronic structure at a given temperature and within a given energy region. Thus, to get insight into the electronic structure of the sample, optical absorption studies have also been accompanied that will be discussed in the upcoming section.

B. Temperature variation of bandgap—GaN

As per the discussion up to this point, it has been understood that the signature of electron-phonon interactions could be probed through the Raman spectroscopy technique where the parameters like lineshape and width associated with a given phonon mode could give information about the strength of EPC [47]. Moreover, it is also known that electron-phonon interactions may affect the electrons due to their participation in the process. Thus, the electronic structure may also be expected to acquire some modifications within the narrow energy region where the energetic overlapping of electrons and phonons is favorable [46,54–56]. Further, since this narrow energy region could exist nearly above the Fermi level, where the electrons may be assumed to become just free enough to interact with nearby phonons, the impact of such an interaction may appear as an optical bandgap renormalization [57]. In other words, as the sample temperature varies, the population of electrons near the Fermi level may also change, thereby affecting the strength of the overall EPC which may reflect in the corresponding variation in the bandgap since

phonons are known to participate in the formation of the absorption edge [40,58]. In that view, TD optical absorption spectra (OAS) have been obtained for the GaN sample from 303 to 423K.

Furthermore, to extract the information of the TD optical bandgap, the Tauc plot for the spectra at that temperature has been obtained. A schematic for the OAS and related Tauc plot at 303 K is shown in Fig. 3(a). The term $F(R)$ denotes the Kubelka-Munk function which is related to the absorption coefficient of the material [59,60]. The dependence of $F(R)$ on incident photon energy ($h\nu$) could be understood as the following [61,62]:

$$F(R) \propto \alpha \propto \frac{(h\nu - E_g)^{1/n}}{h\nu}, \qquad (19)$$

where E_g is the bandgap of the sample, and the number n is related to the nature of the electronic transition occurring in the system ($n = 2, \frac{1}{2}$ for direct, indirect bandgap materials). As GaN is a direct bandgap semiconductor, $n = 2$ has been followed in this paper [63].

Further, the obtained values of E_g have been plotted against temperature in Fig. 3(b), which can be clearly seen to systematically decrease with temperature. To further analyze the temperature variation of E_g in GaN, the Varshni relation [64] [Eq. (20)] has been considered:

$$E_g(T) = E_g(0) - \frac{\alpha T^2}{\beta + T}. \qquad (20)$$

Here, $E_g(0)$ is the bandgap at 0 K, and α and β are the Varshni coefficients. The values of these parameters obtained for the best fit with the experimental data are also listed in the Fig. 3(b), which agree with the earlier reported values [65]. It is noteworthy here that, since the variation in E_g for a given temperature interval could be very sensitive and is a crucial quantity from the perspective of this paper, the E_g values corresponding to the fitted curve have been considered instead of direct experimental values to minimize the deviation/error. This could be further helpful in determining the coupling strength in accordance with Eq. (18).
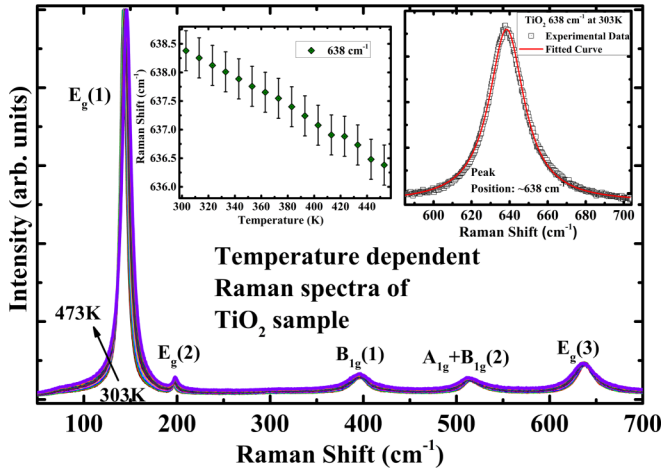
FIG. 4. Temperature-dependent Raman spectra of anatase TiO$_2$ sample collected in range 303–473 K.

C. Temperature variation of Raman and OAS collected for the TiO$_2$ sample

To extend the approach for exploring the mode-specific EPC to an additional system, a polycrystalline TiO$_2$ sample has been considered. The TD Raman and OAS have been shown in the Figs. 4 and 5, respectively. The Raman spectra confirm the anatase phase of the TiO$_2$ sample [64,66], of which the temperature variations of the modes appearing at 144 cm^{-1} (E_g), 196 cm^{-1} (E_g), 398 cm^{-1} (B_{1g}), 515 cm^{-1} ($A_{1g} + B_{1g}$), and 638 cm^{-1} (E_g) have been considered [66,67] in the range of 303–473K. These were then fitted for precisely obtaining the peak positions of the respective modes. The schematics for the fitting at room temperature and the temperature variation of the values of the peak position thus extracted for the E_g(3) mode (~ 638 cm^{-1}) have been provided as the insets of Fig. 4.

A similar process has been carried out to obtain the values of the peak position of the rest of the modes at higher temperatures which would be utilized for obtaining the coupling strength associated with each phonon-mode described by Eq. (18).

For that, the temperature variation of the bandgap for TiO$_2$ is obtained in Fig. 5(b) fitted with the Varshni relation. The values corresponding to the best fit are also mentioned. These values have been used to estimate ΔE_g in accordance with Eq. (18) and hence to obtain the values of phonon-mode-specific coupling constant α_p.

V. MODE-SELECTIVE COUPLING—EXPERIMENTAL INVESTIGATION

So far, a possible connection between the variation in the optical bandgap and EPC strength associated with a given phonon mode has been discussed, which in accordance with Eq. (18) could provide a dimensionless parameter that may be equivalent to the coupling strength for that phonon inferring that each phonon mode could have unique coupling strength with the electrons so that their contribution to the bandgap variation may reflect. Moreover, rewriting Eq. (18):

$$\alpha_p \sim \frac{\Delta E_g}{\hbar \omega_p}. \tag{21}$$

It appears from Eq. (21), those phonons could couple more which lie relatively at lower ω_p which can be understood as the fact that an effective energetic overlap of the electrons with phonons may be favorable for the electronic states lying just above the Fermi level so that the electrons may interact with nearby phonons; hence, phonons existing in this narrow energy region could have relatively lower ω_p. This explains the coupling strength of those phonons at a given temperature. However, the role of the DOS of both electrons (DOS-e) and phonons (DOS-ph) could also be an additional factor to decide the coupling strength [8,49]. This could be understood by applying an external perturbation (temperature, in this case) that may modify the effective energy overlap between electrons and phonons; consequently, the coupling strength may change. Thus, with this concept, it could be explained that different phonon modes, even having higher/lower α, may exhibit a different extent of variation in α depending on the effective overlap of DOS-e/DOS-ph, leading to modification in the coupling strength. Therefore, this paper has been employed over two different optical modes (namely, A_1 and E_2^2)
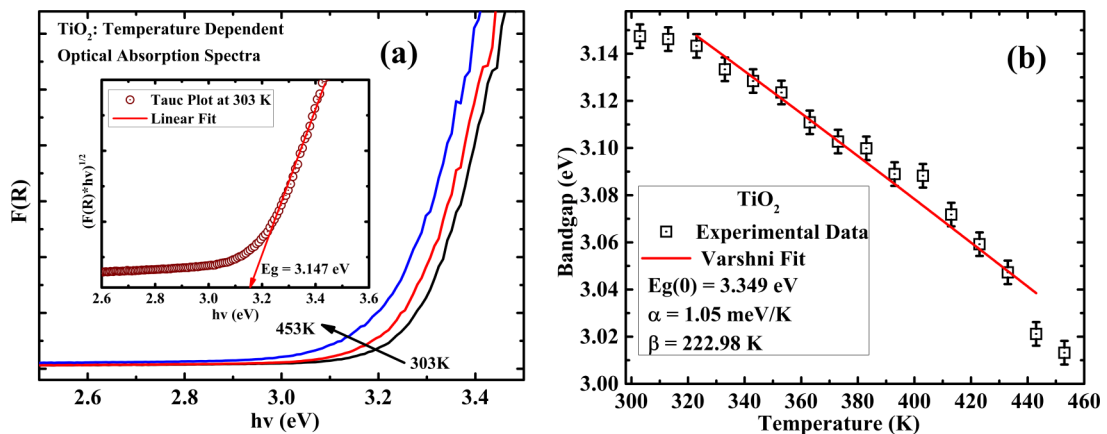
FIG. 5. (a) Schematic representation of the temperature-dependent optical absorption spectra of TiO$_2$ sample and the Tauc plot (inset) at 303 K. (b) Temperature variation of optical bandgap of TiO$_2$ fitted with Varshni relation.
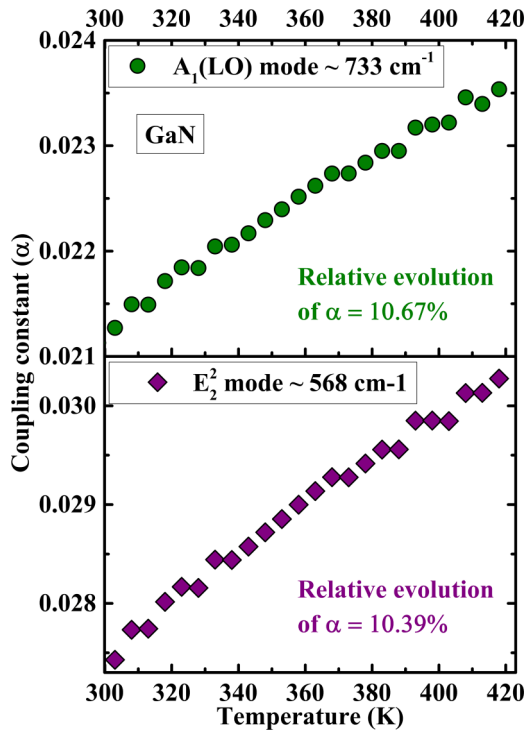
FIG. 6. Plot for the variation of coupling constant (α) as a function of temperature for the A_1(LO) and E_2^2 phonon modes of GaN sample.

occurring in GaN, and the values of α for the two modes have been observed at individual temperatures (see Fig. 6) which provides the information of relative modification in the EPC strength for individual phonon modes. For this, the difference in the bandgap ($\Delta E_g = E_{g1} - E_{g2}$) corresponding to the considered temperature interval ($T_2 - T_1 = 5$ K, for GaN; $T_2 > T_1$) has been utilized to acquire the value of α corresponding to a phonon mode occurring at ω_p (ω_{p1}).

It could be seen that α shows a monotonous increment with the sample temperature such that it has magnitudes of 0.027 and 0.021 for E_2^2 and A_1(LO) modes, respectively, at 298 K, which reach 0.030 (E_2^2) and 0.024 [A_1(LO)] for the respective modes at 418 K, which agrees with the fact that the coupling strength may enhance with the temperature [47]. The E_2^2 mode, being relatively lower in position than the A_1(LO) mode, acquires a larger value of α which may be attributed to the effective overlapping of the E_2^2 mode with the nearby electrons, which may be favored by larger density of interacting electrons and phonons. Nevertheless, the variation in the coupling strength (α) with respect to temperature may be different for the modes due to the alteration in the overlapping of the electronic and phononic states. Therefore, to have further insight into the evolution of EPC associated with the modes, the relative (%) changes in α have been obtained in the considered temperature range which are found to be $\sim$10.39% (E_2^2) and $\sim$10.67% [A_1(LO) mode]. It clearly indicates the preferential coupling of LO phonon over the other phonon mode.

Furthermore, the same approach has also been extended on the polycrystalline TiO_2 sample. The values of the coupling constant (α) found in temperature range 303–473 K

($T_2 - T_1 = 10$ K; $T_2 > T_1$) are depicted in Fig. 7(a) along with the relative average changes (%).

To compare the relative average variations, a more direct insight into the electron-phonon interactions has been further considered over the Raman spectra by estimating the asymmetry parameter $1/|q|$ [47,68,69] of each mode at 473 K [Fig. 7(b)] in accordance with the Fano resonance model [47], as at the higher temperature, EPC may have greater strength due to thermal disorder [47]. It could be realized from the Raman spectra of TiO_2 (Fig. 4) that the Raman mode exhibiting a symmetric profile (lower $1/|q|$) possesses lower average variation in the coupling constant [Fig. 7(b)], attributing to the mode-specific coupling of phonons with the electrons. The observed results for α are also found to be consistent with earlier reports on EPC [17,70].

In this way, our theoretical execution is in good agreement with the experimental evaluations of GaN and TiO_2 samples. Thus, in this paper, we report the simultaneous application of Raman and optical spectroscopies to efficiently probe the coupling strength of individual phonons with electrons in semiconductors.

VI. CONCLUSIONS

In conclusion, a quantitative picture for the electron-phonon interactions in semiconductors was provided via theoretical discussions on polaron model, giving the coupling constant (α) for each phonon mode that was experimentally investigated of GaN and TiO_2 by the bandgap and phonon frequency values at different temperatures. The results obtained according to the discussed model suggest that, in GaN, the LO phonon mode ~ 733 cm^{-1} exhibits a comparatively greater percent increment in α with temperature, which is evident from the preferential coupling of the LO mode. Further, in the case of TiO_2, those modes are found to possess symmetric lineshapes which show smaller percent change in α, attributing to weaker coupling of those modes. This experimental outcome supports the validity of the inferences on phonon-mode-specific α provided in this paper. In this paper, we utilize Raman and optical spectroscopies to probe the phonon-specific coupling which otherwise is obtained via advanced techniques.

All data used for the analyses are available in this paper. Any additional relevant data related to this paper could be made available on request.
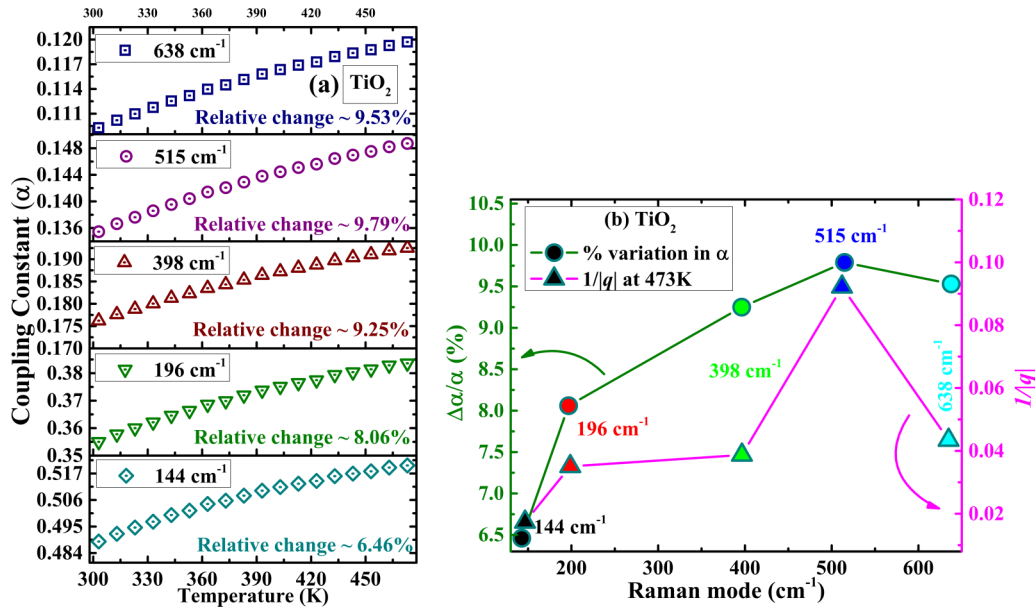
FIG. 7. (a) Variation of α for specific modes of TiO_2 sample with respect to temperature. (b) Comparison of the trend of percent relative change in α with the asymmetry parameter $1/|q|$ (at 473 K) for all modes.

[1] J. M. Ziman, *Electrons and Phonons: The Theory of Transport Phenomena in Solids* (Oxford University Press, Oxford, 2001).

[2] F. Giustino, Electron-phonon interactions from first principles, Rev. Mod. Phys. **89**, 015003 (2017).

[3] J. Bardeen, L. N. Cooper, and J. R. Schrieffer, Theory of superconductivity, Phys. Rev. **108**, 1175 (1957).

[4] V. Ambegaokar and L. Tewordt, Theory of the electronic thermal conductivity of superconductors with strong electron-phonon coupling, Phys. Rev. **134**, A805 (1964).

[5] K. R. Babu and G.-Y. Guo, Electron-phonon coupling, superconductivity, and nontrivial band topology in NbN polytypes, Phys. Rev. B **99**, 104508 (2019).

[6] A. Rubino, A. Francisco-López, A. J. Barker, A. Petrozza, M. E. Calvo, A. R. Goñi, and H. Míguez, Disentangling electron-phonon coupling and thermal expansion effects in the band gap renormalization of perovskite nanocrystals, J. Phys. Chem. Lett. **12**, 569 (2021).

[7] N. W. Ashcroft and N. D. Mermin, *Solid State Physics* (Holt, Rinehart and Winston, New York, 1976).

[8] F. C. Yang, O. Hellman, and B. Fultz, Temperature dependence of electron-phonon interactions in vanadium, Phys. Rev. B **101**, 094305 (2020).

[9] X. Zhou, L. Li, H. Dong, A. Giri, P. E. Hopkins, and O. V. Prezhdo, Temperature dependence of electron-phonon interactions in gold films rationalized by time-domain *ab initio* analysis, J. Phys. Chem. C **121**, 17488 (2017).

[10] U. Fano, Effects of configuration interaction on intensities and phase shifts, Phys. Rev. **124**, 1866 (1961).

[11] F. Cerdeira, T. A. Fjeldly, and M. Cardona, Effect of free carriers on zone-center vibrational modes in heavily doped *p*-type Si. II. Optical modes, Phys. Rev. B **8**, 4734 (1973).

[12] A. W. Bushmaker, V. V. Deshpande, M. W. Bockrath, and S. B. Cronin, Direct observation of mode selective electron-phonon coupling in suspended carbon nanotubes, Nano Lett. **7**, 3618 (2007).

[13] D. H. Lee, S.-J. Choi, H. Kim, Y.-S. Kim, and S. Jung, Direct probing of phonon mode specific electron-phonon scatterings in two-dimensional semiconductor transition metal dichalcogenides, Nat. Commun. **12**, 4520 (2021).

[14] O. Celik, E. Tiras, S. Ardali, S. Lisesivdin, and E. Ozbay, Determination of the LO phonon energy by using electronic and optical methods in AlGaN/GaN, Cent. Eur. J. Phys. **10**, 485 (2012).

[15] M. X. Na, A. K. Mills, F. Boschini, M. Michiardi, B. Nosarzewski, R. P. Day, E. Razzoli, A. Sheyerman, M. Schneider, G. Levy *et al.*, Direct determination of mode-projected electron-phonon coupling in the time domain, Science **366**, 1231 (2019).

[16] S. D. Brorson, A. Kazeroonian, J. S. Moodera, D. W. Face, T. K. Cheng, E. P. Ippen, M. S. Dresselhaus, and G. Dresselhaus, Femtosecond Room-Temperature Measurement of the Electron-Phonon Coupling Constant Γ in Metallic Superconductors, Phys. Rev. Lett. **64**, 2172 (1990).

[17] I. Yu. Sklyadneva, G. Benedek, E. V. Chulkov, P. M. Echenique, R. Heid, K.-P. Bohnen, and J. P. Toennies, Mode-Selected Electron-Phonon Coupling in Superconducting Pb Nanofilms Determined from He Atom Scattering, Phys. Rev. Lett. **107**, 095502 (2011).

[18] S. Moser, S. Fatale, P. Krüger, H. Berger, P. Bugnon, A. Magrez, H. Niwa, J. Miyawaki, Y. Harada, and M. Grioni, Electron-Phonon Coupling in the Bulk of Anatase TiO_2 Measured by Resonant Inelastic X-Ray Spectroscopy, Phys. Rev. Lett. **115**, 096404 (2015).

[19] C. G. Kuper and G. D. Whitfield, Introduction to the theory of the polaron, in *Polarons and Excitons*, edited by H. Frohlich (Plenum, New York, 1963), pp. 1–28.

[20] M. A. Smondyrev, Diagrams in the polaron model, Theor. Math. Phys. **68**, 653 (1986).

[21] J. T. Devreese, Fröhlich polarons. Lecture course including detailed theoretical derivations, arXiv:1012.4576 (2010).

[22] T. J. Flack, B. N. Pushpakaran, and S. B. Bayne, GaN technology for power electronic applications: A review, J. Electron. Mater. **45**, 2673 (2016).

[23] M. Park, J. J. Cuomo, B. J. Rodriguez, W.-C. Yang, R. J. Nemanich, and O. Ambacher, Micro-Raman study of electronic properties of inversion domains in GaN-based lateral polarity heterostructures, J. Appl. Phys. **93**, 9542 (2003).

[24] M. Kawase and J. Suda, Temperature dependence of the local electronic properties of n-type GaN crystals by micro-Raman spectroscopy and dielectric dispersion at high temperatures, Jpn. J. Appl. Phys. **60**, 048002 (2021).

[25] A. P. Vajpeyi, S. Tripathy, S. J. Chua, and E. A. Fitzgerald, Investigation of optical properties of nanoporous GaN films, Phys. E: Low-Dimens. Syst. Nanostructures **28**, 141 (2005).

[26] D. Y. Song, M. Basavaraj, S. A. Nikishin, M. Holtz, V. Soukhoveev, A. Usikov, and V. Dmitriev, The influence of phonons on the optical properties of GaN, J. Appl. Phys. **100**, 113504 (2006).

[27] E. Estephan, C. Larroque, F. J. G. Cuisinier, Z. Bálint, and C. Gergely, Tailoring GaN semiconductor surfaces with biomolecules, J. Phys. Chem. B **112**, 8799 (2008).

[28] F. Sarikhani, A. Zabardasti, A. R. Soleymani, and M. Naseri, Enhanced visible light activity of $EuFeO_3/TiO_2$ nanocomposites prepared by thermal treatment–hydrolysis precipitation method, Appl. Phys. A **126**, 476 (2020).

[29] S. Wu, Z. Weng, X. Liu, K. W. K. Yeung, and Paul. K. Chu, Functionalized TiO_2 based nanomaterials for biomedical applications, Adv. Funct. Mater. **24**, 5464 (2014).

[30] Y. Zhang, Z.-R. Tang, X. Fu, and Y.-J. Xu, TiO_2-graphene nanocomposites for gas-phase photocatalytic degradation of volatile aromatic pollutant: Is TiO_2-graphene truly different from other TiO_2-carbon composite Materials? ACS Nano **4**, 7303 (2010).

[31] T.-X. Qin, E.-M. You, J.-Y. Zhang, H.-L. Wang, K. H. L. Zhang, B.-W. Mao, and Z.-Q. Tian, Revealing the interaction of charge carrier–phonon coupling by quantification of electronic properties at the $SrTiO_3/TiO_2$ heterointerface, Nano Lett. **22**, 2755 (2022).

[32] T. K. Mitra, A. Chatterjee, and S. Mukhopadhyay, Polarons, Phys. Rep. **153**, 91 (1987).

[33] M. Gupta, O. V. Rambadey, A. Sagdeo, and P. R. Sagdeo, Investigating the structural, vibrational, optical, and dielectric properties in Mg-substituted $LaAlO_3$, J. Mater. Sci.: Mater. Electron **33**, 13352 (2022).

[34] M. Gupta, O. V. Rambadey, and P. R. Sagdeo, Probing the effect of R-cation radii on structural, vibrational, optical, and dielectric properties of rare earth (R = La, Pr, Nd) aluminates, Ceram. Int. **48**, 23072 (2022).

[35] A. Kumar, M. K. Warshi, A. Sagdeo, M. Gupta, and P. R. Sagdeo, New route to estimate the Mott-Hubbard and charge transfer parameters: An optical and x-ray absorption studies, Solid State Sci. **115**, 106582 (2021).

[36] V. Mishra, M. K. Warshi, R. Kumar, and P. R. Sagdeo, Design and development of *in-situ* temperature dependent diffuse reflectance spectroscopy setup, J. Instrum. **13**, T11003 (2018).

[37] A. Kumar, S. Umrao, and P. R. Sagdeo, Orbital facilitated charge transfer originated phonon mode in Cr-substituted $PrFeO_3$: A brief Raman study, J. Raman Spectrosc. **51**, 1210 (2020).

[38] M. K. Warshi, A. Kumar, A. Sati, S. Thota, K. Mukherjee, A. Sagdeo, and P. R. Sagdeo, Cluster glass behavior in orthorhombic $SmFeO_3$ perovskite: Interplay between spin ordering and lattice dynamics, Chem. Mater. **32**, 1250 (2020).

[39] M. Gupta, S. C. Shirbhate, O. V. Rambadey, S. A. Acharya, and P. R. Sagdeo, Temperature-dependent delocalization of oxygen vacancies in La-substituted CeO_2, ACS Appl. Energy Mater. **5**, 9759 (2022).

[40] O. V. Rambadey, A. Kumar, K. Kumar, V. Mishra, and P. R. Sagdeo, Methodology to probe disorder contribution in Raman linewidth via optical absorption spectroscopy in orthoferrite $EuFeO_3$, J. Phys. Chem. C **126**, 13946 (2022).

[41] A. Kumar, M. K. Warshi, A. Sagdeo, M. Krzystyniak, S. Rudić, D. T. Adroja, I. da Silva, and P. R. Sagdeo, Origin of natural and magnetic field induced polar order in orthorhombic $Pr Fe_{1/2}Cr_{1/2}O_3$, Phys. Rev. B **104**, 035101 (2021).

[42] A. Kumar, O. V. Rambadey, H. Rai, and P. R. Sagdeo, Role of laser excitation wavelength and power in the Fano resonance scattering in $RFe_{0.50}Cr_{0.50}O_3$ (R = Sm, Er, and Eu): A brief Raman study, J. Phys. Chem. C **126**, 5403 (2022).

[43] H. Mishra, A. Bose, A. Dhar, and S. Bhattacharya, Exciton-phonon coupling and band-gap renormalization in monolayer WSe_2, Phys. Rev. B **98**, 045143 (2018).

[44] F. Karsai, M. Engel, E. Flage-Larsen, and G. Kresse, Electron-phonon coupling in semiconductors within the GW approximation, New J. Phys. **20**, 123008 (2018).

[45] C. Ablitt, S. Craddock, M. S. Senn, A. A. Mostofi, and N. C. Bristowe, The origin of uniaxial negative thermal expansion in layered perovskites, npj Comput. Mater. **3**, 44 (2017).

[46] J. Bhosale, A. K. Ramdas, A. Burger, A. Muñoz, A. H. Romero, M. Cardona, R. Lauck, and R. K. Kremer, Temperature dependence of band gaps in semiconductors: Electron-phonon interaction, Phys. Rev. B **86**, 195208 (2012).

[47] O. V. Rambadey, A. Kumar, and P. R. Sagdeo, Investigating the correlation between the Urbach energy and asymmetry parameter of the Raman mode in semiconductors, Phys. Rev. B **104**, 245205 (2021).

[48] C. F. Klingshirn, *Semiconductor Optics* (Springer, Berlin, Heidelberg, 2012), Chap. 8.

[49] O. Delaire, M. Kresch, J. A. Muñoz, M. S. Lucas, J. Y. Y. Lin, and B. Fultz, Electron-phonon interactions and high-temperature thermodynamics of vanadium and its alloys, Phys. Rev. B **77**, 214112 (2008).

[50] M. Gopalakrishnan, V. Purushothaman, P. S. Venkatesh, V. Ramakrishnan, and K. Jeganathan, Structural and optical properties of GaN and InGaN nanoparticles by chemical Co-precipitation method, Mater. Res. Bull. **47**, 3323 (2012).

[51] A. Kumar, V. Mishra, M. K. Warshi, A. Sati, A. Sagdeo, R. Kumar, and P. R. Sagdeo, Strain induced disordered phonon modes in Cr doped PrFeO₃, J. Phys. Condens. Matter **31**, 275602 (2019).

[52] M. Balkanski, R. F. Wallis, and E. Haro, Anharmonic effects in light scattering due to optical phonons in silicon, Phys. Rev. B **28**, 1928 (1983).

[53] G. J. Ackland, High-pressure phases of group IV and III-V semiconductors, Rep. Prog. Phys. **64**, 483 (2001).

[54] S. Gopalan, P. Lautenschlager, and M. Cardona, Temperature dependence of the shifts and broadenings of the critical points in GaAs, Phys. Rev. B **35**, 5577 (1987).

[55] S. Zollner, M. Cardona, and S. Gopalan, Isotope and temperature shifts of direct and indirect band gaps in diamond-type semiconductors, Phys. Rev. B **45**, 3376 (1992).

[56] S. Logothetidis, J. Petalas, H. M. Polatoglou, and D. Fuchs, Origin and temperature dependence of the first direct gap of diamond, Phys. Rev. B **46**, 4483 (1992).

[57] G. Antonius, S. Poncé, P. Boulanger, M. Côté, and X. Gonze, Many-Body Effects on the Zero-Point Renormalization of the Band Structure, Phys. Rev. Lett. **112**, 215501 (2014).

[58] A. Kumar, M. K. Warshi, V. Mishra, S. K. Saxena, R. Kumar, and P. R. Sagdeo, Strain control of Urbach energy in Cr-doped PrFeO₃, Appl. Phys. A **123**, 576 (2017).

[59] O. V. Rambadey, A. Kumar, A. Sati, and P. R. Sagdeo, Exploring the interrelation between Urbach energy and dielectric constant in Hf-substituted BaTiO₃, ACS Omega **6**, 32231 (2021).

[60] A. Kumar, O. V. Rambadey, and P. R. Sagdeo, Unorthodox approach to realize the correlation between the dielectric constant and electronic disorder in Cr-doped PrFeO₃, J. Phys. Chem. C **125**, 7378 (2021).

[61] M. K. Warshi, V. Mishra, A. Sagdeo, V. Mishra, R. Kumar, and P. R. Sagdeo, Structural, optical and electronic properties of RFeO₃, Ceram. Int. **44**, 8344 (2018).

[62] A. Sati, V. Mishra, A. Kumar, M. Warshi, A. Sagdeo, R. Kumar, and P. Sagdeo, Effect of structural disorder on the electronic and phononic properties of Hf doped BaTiO₃, J. Mater. Sci. Mater. Electron. **30**, 9498 (2019).

[63] B.-M. Ming, R.-Z. Wang, C.-Y. Yam, L.-C. Xu, W.-M. Lau, and H. Yan, Bandgap engineering of GaN nanowires, AIP Adv. **6**, 055018 (2016).

[64] V. Mishra, M. K. Warshi, A. Sati, A. Kumar, V. Mishra, R. Kumar, and P. R. Sagdeo, Investigation of temperature-dependent optical properties of TiO2 using diffuse reflectance spectroscopy, SN Appl. Sci. **1**, 241 (2019).

[65] C. Prall, M. Ruebesam, C. Weber, M. Reufer, and D. Rueter, Photoluminescence from GaN layers at high temperatures as a candidate for *in situ* monitoring in MOVPE, J. Cryst. Growth **397**, 24 (2014).

[66] S. Challagulla, K. Tarafder, R. Ganesan, and S. Roy, Structure sensitive photocatalytic reduction of nitroarenes over TiO₂, Sci. Rep. **7**, 8783 (2017).

[67] M. Giarola, A. Sanson, F. Monti, G. Mariotto, M. Bettinelli, A. Speghini, and G. Salviulo, Vibrational dynamics of anatase TiO₂: Polarized Raman spectroscopy and *ab initio* calculations, Phys. Rev. B **81**, 174305 (2010).

[68] M. Gupta, A. Kumar, A. Sagdeo, and P. R. Sagdeo, Doping-induced combined Fano and phonon confinement effect in La-doped CeO₂: Raman spectroscopy analysis, J. Phys. Chem. C **125**, 2648 (2021).

[69] A. Kumar, A. Sati, V. Mishra, M. K. Warshi, R. Kumar, and P. R. Sagdeo, Charge neutral crystal field transitions: A measure of electron-phonon interaction, J. Phys. Chem. Solids **135**, 109102 (2019).

[70] P. Ji and Y. Zhang, *Ab initio* determination of effective electron-phonon coupling factor in copper, Phys. Lett. A **380**, 1551 (2016).